AIP Journal of
Renewable and Sustainable Energy

Photovoltaic properties of thin film heterojunctions with cupric oxide absorber

T. Dimopoulos, A. Peić, P. Müllner, M. Neuschitzer, R. Resel et al.

Citation: J. Renewable Sustainable Energy **5**, 011205 (2013); doi: 10.1063/1.4791779

View online: http://dx.doi.org/10.1063/1.4791779

View Table of Contents: http://jrse.aip.org/resource/1/JRSEBH/v5/i1

Published by the AIP Publishing LLC.

Additional information on J. Renewable Sustainable Energy

Journal Homepage: http://jrse.aip.org/

Journal Information: http://jrse.aip.org/about/about_the_journal

Top downloads: http://jrse.aip.org/features/most_downloaded

Information for Authors: http://jrse.aip.org/authors

ADVERTISEMENT

AIP Journal of Renewable and Sustainable Energy
Sign Up For the Free Newsletter Today!
AIP Journal of Renewable and Sustainable Energy

JOURNAL OF RENEWABLE AND SUSTAINABLE ENERGY **5**, 011205 (2013)

Photovoltaic properties of thin film heterojunctions with cupric oxide absorber

T. Dimopoulos,[1,a)] A. Peić,[1] P. Müllner,[1] M. Neuschitzer,[2] R. Resel,[2]
S. Abermann,[3] M. Postl,[4] E. J. W. List,[2,4] S. Yakunin,[5] W. Heiss,[5]
and H. Brückl[1]
[1]*Health and Environment Department, Austrian Institute of Technology, Donau-City Str. 1, 1220 Vienna, Austria*
[2]*Institute of Solid State Physics, Graz University of Technology, Petersgasse 16, 8010 Graz, Austria*
[3]*Energy Department, Austrian Institute of Technology, Giefinggasse 2, 1210 Vienna, Austria*
[4]*NanoTecCenter Weiz Forschungsgesellschaft mbH, Franz-Pichler-Str. 32, 8160 Weiz, Austria*
[5]*Institute for Semiconductor and Solid State Physics, Johannes Kepler University, Altenbergerstr. 69, 4040 Linz, Austria*

(Received 9 September 2012; accepted 26 November 2012; published online 27 February 2013)

In this work, we report on the fabrication, characterization, and photovoltaic properties of sputter-deposited, thin film heterojunctions combining p-type cupric oxide (CuO) absorber with n-type ZnO. The structural investigation reveals highly crystalline, columnar growth of the layers and confirms that the absorber's phase is purely CuO, with only negligible traces of Cu_2O. The optical characterization yields for CuO an indirect bandgap of 1.2 eV and a direct optical transition at approximately 3 eV. The short circuit current, open circuit voltage, fill factor, and power conversion efficiency of the heterojunction solar cells were extracted as a function of the CuO thickness under AM1.5 G (1 kW/m^2) illumination. From the observed dependencies, we conclude that the photovoltaic performance is compromised by a restricted carrier collection efficiency, caused by the small carrier lifetime in CuO. Indeed, the carrier population is found to decay with time constants of 40 and 460 ps. A maximum power conversion efficiency of 0.08% was obtained for the solar cell with CuO thickness of 500 nm. © *2013 American Institute of Physics*. [http://dx.doi.org/10.1063/1.4791779]

I. INTRODUCTION

Copper-oxide semiconductors, namely cuprous (Cu_2O) and cupric (CuO) oxide, are earth-abundant, low-cost, and of low environmental impact. Both materials show intrinsic p-type conductivity. Cu_2O has a direct band-gap of 2.0 eV and CuO an indirect one of 1.2 eV. Due to these properties, both materials are considered promising as solar cell absorbers.[1,2] Indeed, Cu_2O is one of the first investigated absorbers, with reported power conversion efficiency, η, up to 3.83%.[3–7] On the other hand, CuO has been investigated as component material in gas sensing devices,[8–11] in photoelectrochemical cells,[12–14] as cathode in dye-sensitized solar cells,[15] or as basis of high temperature superconductors.[16,17] Despite this large application spectrum, CuO was rarely reported as active solar cell absorber in the literature. More specifically, in one case, CuO nanocrystals were combined with an organic compound, achieving efficiency of 0.04%.[18] Photovoltaic effects were also observed in core–shell CuO/C_{60} junctions with estimated efficiency of 0.02% (Ref. 19) and also in thin film heterojunctions of the same type with efficiency in the order of 10^{-4}%.[20] Finally, the best efficiency of nearly 0.1% was reported for CuO

[a)] Author to whom correspondence should be addressed. Electronic mail: theodoros.dimopoulos@ait.ac.at.

nanowires covered with n-type ZnO.[21] Since the n-type doping of CuO is difficult, heterojunction architectures were implemented in all cases.

In this paper, we investigate the photovoltaic (PV) properties of sputtered, thin film solar cells based on the n-ZnO/p-CuO heterojunction, as a function of the CuO absorber thickness. The observed PV characteristics are discussed in correlation with the intrinsic properties of the CuO absorber.

II. EXPERIMENTAL

The thin films were deposited by magnetron sputtering (Leybold Univex 450C system) on 1 mm-thick microscope slides (Menzel Gläser), cleaned in acetone and isopropanol baths under sonication. During the sputter process, the targets and substrate holder were water-cooled at 25 °C. The target–substrate distance was 10 cm and the sputter chamber base pressure in the range of 7×10^{-6}–1.2×10^{-5} Pa. The deposition parameters of the films are shown in Table I. The film thicknesses and the corresponding sputter rates were extracted from step-height measurements using a surface profiler (Alpha Step IQ).

Scanning electron microscopy (SEM) (Zeiss SUPRA 40 microscope) was used to image the surface morphology and cross sections of the layers. The surface topography of the films was also obtained using an atomic force microscope (AFM) (Molecular Imaging, PicoPlus), operated in the tapping mode. X-ray diffraction (XRD) measurements were carried out either in specular geometry or in grazing incidence surface geometry (GIXD). Specular diffraction was performed with a SIEMENS D501 diffractometer in Bragg-Brentano geometry using a graphite monochromator at the secondary side. GIXD investigations were performed with a Bruker D8 DISCOVER diffractometer specially adapted for surface diffraction.[22] An incident angle of $\alpha_i = 0.15°$ was used for the primary beam. The diffracted beams were detected in an out-of-plane scattering angle α_f between 0° and 7° relative to the substrate surface and plotted as integrated intensities versus the in-plane scattering angle 2θ. The optical transmission properties of the films at normal light incidence were probed using an ultraviolet–visible (UV-VIS) spectrophotometer (Thermo Electron Corporation, Nicolet Evolution 100). Photoluminescence (PL) measurements were conducted on a Shimadzu RF-5301PC spectro-fluoro-photometer at room temperature in air. The film sheet resistance was measured with the four-point, in-line probe technique and current density-voltage (j-V) characteristics were obtained with a semiconductor parameter analyser (Agilent 4156C). Solar cell characteristics under ambient conditions were extracted from the j-V curves under AM1.5 G (1 kW/m^2) illumination.

Apart from single layers sputtered on glass and used for material characterization purposes, heterojunction solar cells were prepared as follows: the glass substrates were covered with a 210 nm Al-doped ZnO (AZO) film (for composition see Table I), with a sheet resistance of 60 Ω. A 100 nm-thick, n-type, intrinsic ZnO layer was then deposited, followed by the p-type CuO absorber. The thickness, x, of the latter varied between 200 and 900 nm. A 20 nm-thick, p-type NiO layer was subsequently sputtered, followed by the deposition of Au contacts through a shadow mask. In the following, the thickness of the films is denoted in parentheses in nm.

TABLE I. List of the sputtering parameters for each material, along with the corresponding deposition rate.

Film	Target	Target diameter (inch)	Power (W)	Gas	Pressure (Pa)	Deposition rate (nm/s)
Al:ZnO (AZO)	ZnO, doped 2 wt. % Al_2O_3	4	160 (DC)	Ar	0.1	0.78
ZnO	ZnO	4	40 (DC)	Ar/O_2: 80/20	1	0.08
CuO	Cu	3	80 (DC)	Ar/O_2: 80/20	2	0.22
NiO	NiO	4	200 (RF)	Ar/O_2: 80/20	0.5	0.04
Au	Au	3	20 (DC)	Ar	0.2	0.32

III. RESULTS AND DISCUSSION

Fig. 1(a) shows a cross section SEM image of a heterojunction solar cell with 900 nm-thick CuO, obtained from a cleaved edge of the sample, prior to Au contact deposition. The difference between the layer thicknesses extracted from the SEM image and the nominal values is less than 3%. In Fig. 1(b), the cross section is depicted in higher magnification, showing the AZO and ZnO films, as well as the lower part of the absorber. AZO and ZnO crystallize in the hexagonal, wurtzite structure. Figs. 1(a) and 1(b) show a pronounced columnar growth for these films. The transition from AZO to ZnO is marked by an increased brightness, caused by the change in film composition and electrical conductivity. ZnO columns grow as extensions of the underlying AZO ones, due to the minimal lattice mismatch between the intrinsic and the doped material ($\sim$1% mismatch). The AZO and ZnO growth along the wurtzite *c*-axis is manifested in the specular, X-ray diffractogram of Fig. 2(a) with a dominant peak, ascribed to the ZnO (002) planes' reflection (the sample description used for the XRD characterization is given in the caption of Fig. 2).

CuO (tenorite) belongs to the prismatic class (2/m) of the monoclinic system. In Figs. 1(a) and 1(b), we observe its growth on top of the ZnO columns. It forms long, vertically oriented, pointed pillars that broaden with increasing layer thickness. The pillar faces are not smooth but consist of fish scale-like crystallites. These morphological features are characteristic for tenorite.[23,24] The cross section SEM images depict a CuO film lacking compactness, as gaps between the pillars are clearly observed. Such a microstructure is generally associated with film deposition at low substrate temperature and low kinetic energy of deposited species.[25] CuO is, indeed, deposited at 25 °C, which favors a void-rich film. Most importantly, the formation mechanism

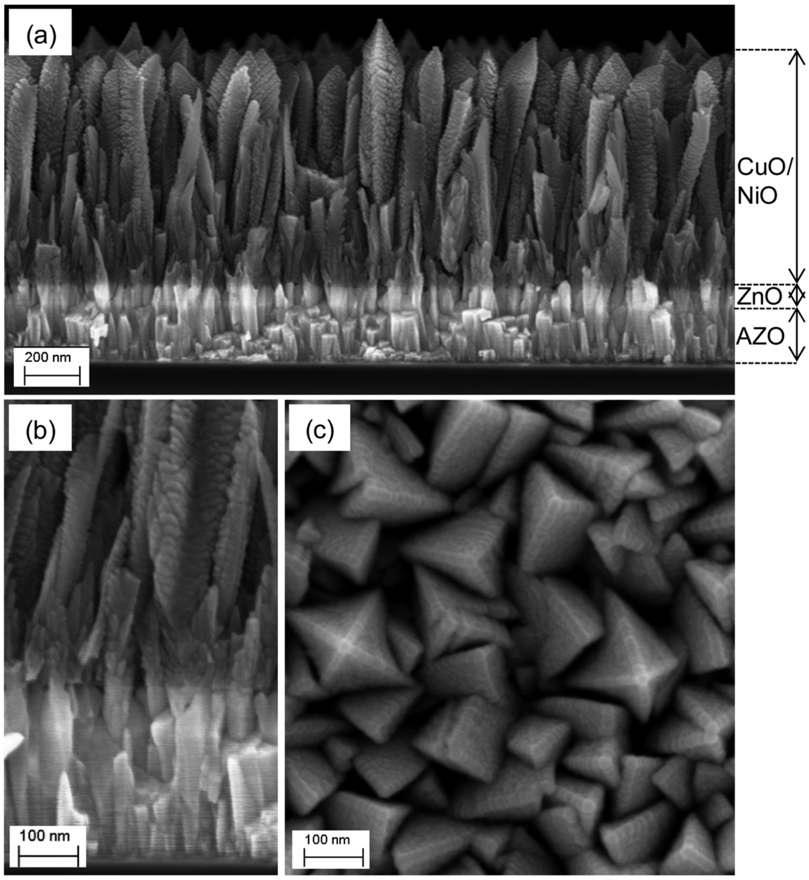

FIG. 1. (a) and (b) Cross section SEM images of the sample: glass/AZO(210)/ZnO(100)/CuO(900)/NiO(20). (c) Top surface SEM image from the same sample.

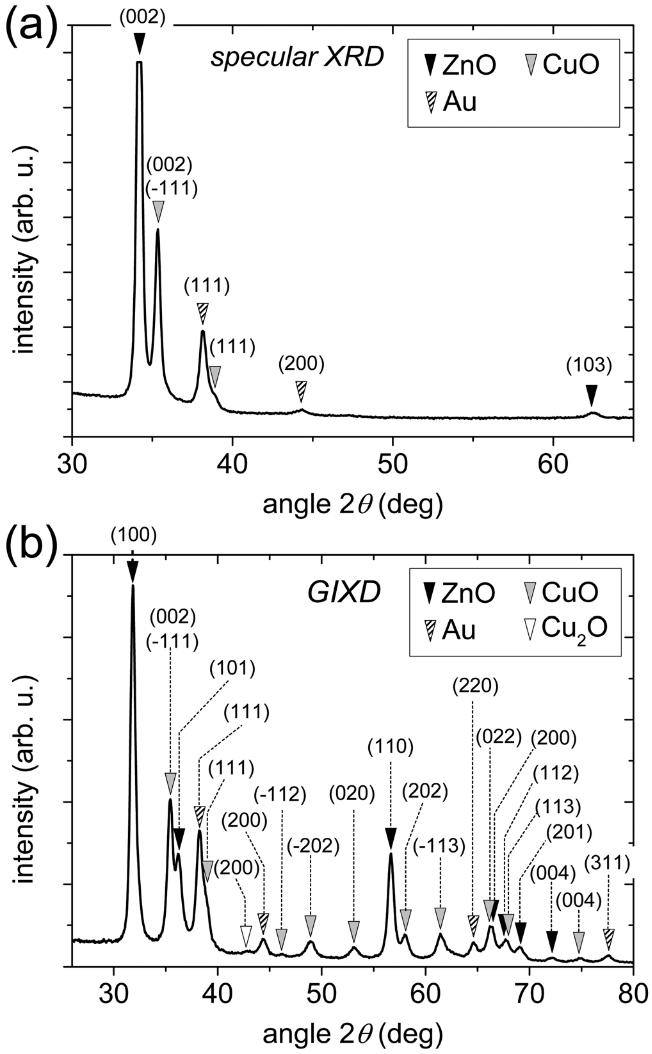

FIG. 2. (a) Specular XRD from the sample: glass/AZO(210)/ZnO(100)/CuO(200)/NiO(20)/Au(50). (b) Grazing incidence surface diffraction from the same sample. The indexation of the diffraction peaks is obtained from reference patterns of polycrystalline materials (database: Powder Diffraction File 2 (PDF2) from the International Center of Diffraction Data (ICDD).

of voids requires the presence of surface roughness.[25] This can explain the fact that CuO films sputtered directly on the smooth glass surface are considerably more compact than films sputtered on the rougher AZO/ZnO electrode. Fig. 1(c) shows the top view of the multilayer, prior to Au contact deposition. We can clearly distinguish the square and triangular pyramids ending the CuO pillars, with well defined edges and fine structure on their faces. Fig. 3 illustrates AFM topography images of heterojunctions with $x = 400\,\mathrm{nm}$ and $x = 900\,\mathrm{nm}$ CuO film thickness, prior to Au deposition. The extracted root-mean-square roughness increased with increasing x from a value of 14.1 nm for $x = 400\,\mathrm{nm}$ to 38.7 nm for $x = 900\,\mathrm{nm}$. The AFM images also clearly demonstrate the broadening of the pillars with increasing CuO thickness. This broadening comes as a consequence of the competitive type of the film's growth, i.e., due to sterical hindrance, crystals with the fastest growth rate gradually develop in all dimensions at the expense of the slower growing ones. Autocorrelation functions (ACF) of the AFM height profiles were calculated to estimate the mean pillar size, d, as the full width at half maximum of the ACF peak. This yielded $d = 54\,\mathrm{nm}$ for $x = 400\,\mathrm{nm}$ and $d = 107\,\mathrm{nm}$ for $x = 900\,\mathrm{nm}$.

The specular XRD (Fig. 2(a)) yields an intense peak stemming from the tenorite (002) and/or (-111) planes (both are expected at practically the same angle position) and a weaker one

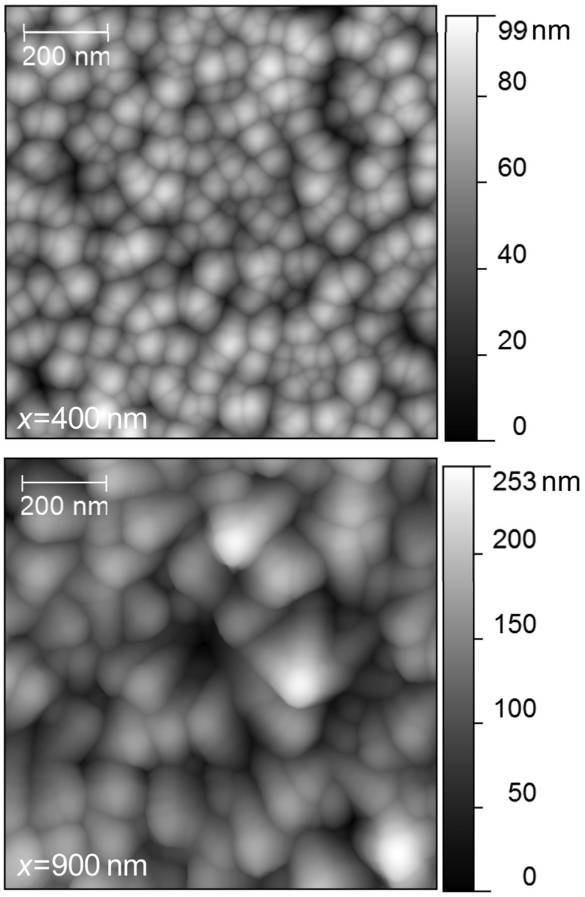

FIG. 3. $1 \times 1\ \mu m^2$ AFM topography images from heterojunctions with $x = 400$ nm and $x = 900$ nm absorber thickness.

due to the (111) planes. Apart from the ZnO and CuO peaks, two peaks stemming from the Au top contacts are also present.

To gain more insight on the possible existence of other copper oxide phases, the sample was also investigated in grazing incidence geometry. The GIXD pattern is shown in Fig. 2(b). A multitude of copper oxide peaks appears in this case, all but one ascribed to the tenorite phase. Again, the most pronounced peak belongs to the tenorite (002) and/or (−111) plane reflection. Only one, very low intensity peak at 42.7° could be identified as belonging to the Cu_2O (200) planes. We note here that the same peaks were obtained for single CuO layers deposited directly on glass. A comparison of the peak intensities of both copper oxide phases (CuO and Cu_2O) reveals that the quantitative fraction of Cu_2O is below few wt. %, which is actually the detection limit for phase analysis.[26] In addition, NiO did not give rise to any XRD peaks, neither for multilayer samples nor for single NiO layers deposited on glass, suggesting that the NiO film is amorphous.

UV-VIS optical transmission spectra for all investigated films are shown in Fig. 4(a). These spectra were used to produce linear fits of the quantity $(\alpha h\nu)^n$ versus $h\nu$ (Tauc plot), where α is the optical absorption, $h\nu$ is the photon energy, and n is an index assuming the value of 2 for direct bandgap and 0.5 for indirect bandgap materials. The fitting yielded direct bandgap values of 3.42, 3.27, and 3.47 eV for AZO, ZnO, and NiO, respectively (Fig. 4(b)). The AZO bandgap is slightly higher than the one of the ZnO due to the Moss-Burstein shift, whereas literature values for the direct bandgap of NiO lie between 3.4 and 4.3 eV.[27–29] For the CuO absorber, a straight line relationship is obtained when $(\alpha h\nu)^{0.5}$ is plotted against photon energy (Fig. 4(c)), indicating that the absorption edge is due to an indirect bandgap. The extracted value of 1.2 eV is in good agreement with the photo-electrochemical bandgap determination from Koffyberg

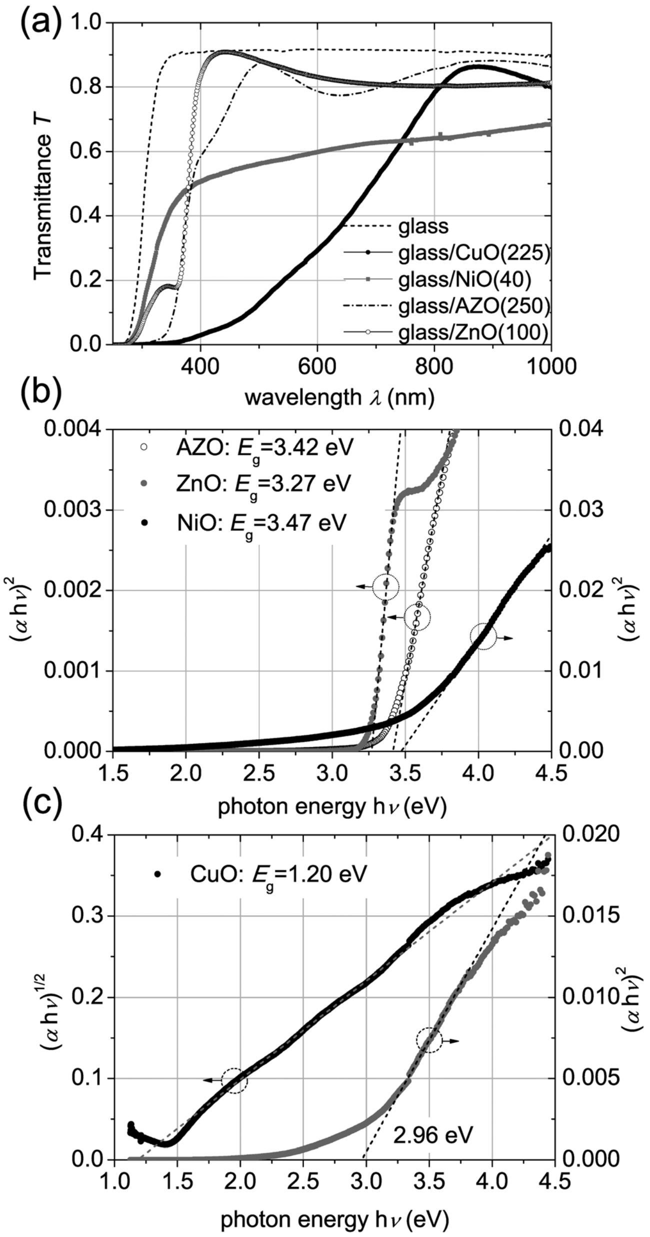

FIG. 4. (a) UV-VIS measurements of the transmittance, T, versus wavelength, λ, for normal light incidence. (b) Extraction of the direct bandgap of AZO, ZnO, and NiO. (c) Extraction of the CuO indirect bandgap (full black dots) and of the direct optical transition gap (full grey dots).

and Benko at 1.35 eV (Ref. 30) and with the electronic band-structure calculations from Wu and Zhang,[31] who obtained a value of 1.0 eV. The indirect bandgap originates from Cu-3d orbitals forming the two bottom conduction bands and the top valence band.[31] In Fig. 4(c), we also plot for CuO the quantity $(\alpha h\nu)^2$ versus hν. The obtained linear fit suggests a direct allowed interband transition in CuO of approximately 3 eV, a bit short of the 3.25 eV reported in Ref. 30. This transition was claimed to arise from the low lying oxygen-2p band to the conduction band.[30] The PL spectrum of a single CuO layer (Fig. 5), excited with a 240 nm light source, shows an asymmetric peak with its maximum at 380 nm (3.26 eV) and a bump at its right flank, at 405 nm (3.06 eV). These features are consistent with the results of Ref. 30 and our extraction of the direct transition from the UV-VIS measurements.

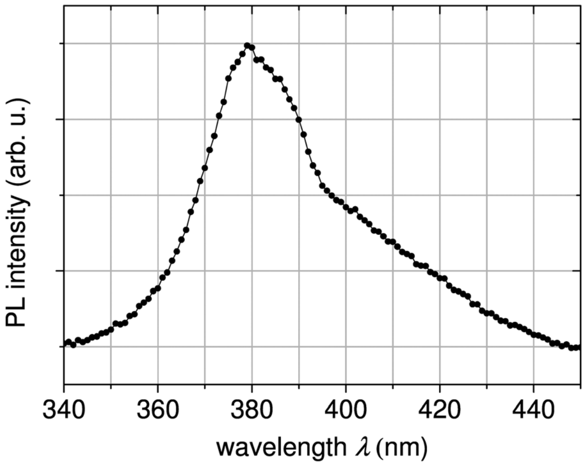

FIG. 5. Photoluminescence spectrum measured for a single, 200 nm-thick CuO layer on glass, with an excitation wavelength of 240 nm.

For the CuO film, a resistivity of 24 Ω cm was measured. Literature values for the CuO resistivity span from 16 to 1000 Ω cm, depending on the fabrication process and the presence of doping.[30,32,33] The undoped CuO is dominated by stable copper vacancies, which give rise to the intrinsic p-type conductivity.[31] The NiO film, also an intrinsic p-type semiconductor, yielded a resistivity of 40 Ω cm and the intrinsic ZnO exhibited nearly insulating behavior with a resistivity of more than 5×10^6 Ω cm.

Fig. 6 depicts the energy band diagram of the CuO-based solar cell, taking into account the materials' electron affinity values from the literature[30,35,36] and the bandgap values extracted from the measurements. The conduction band alignment between CuO and ZnO secures that electrons can be transferred to the ZnO easily and from there to the AZO cathode. The same applies for holes, which are collected at the Au electrode after being transferred to the NiO, whose valence band coincides with the valence band of CuO. Indeed, both CuO and NiO have valence bands made up mainly from the 3*d* atomic wavefunctions of the metal ions.[30] At the same time, NiO serves as electron blocking layer in view of the large difference between its conduction band position and the one of CuO. Indeed, NiO has demonstrated efficiency-enhancing properties as an anode interfacial layer in polymer light-emitting devices and solar cells.[34,35] The sputtered NiO film forms a high quality p-n junction when combined with ZnO,

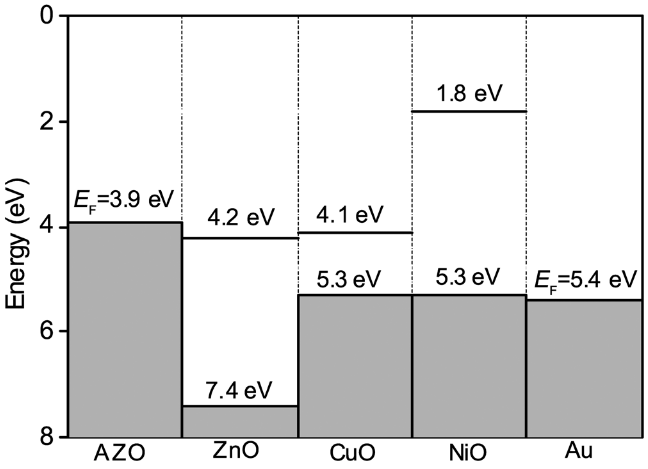

FIG. 6. Energy diagram of the investigated solar cell, assuming vacuum level alignment.

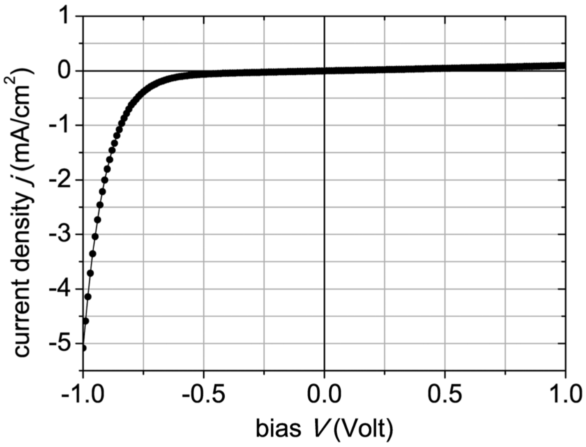

FIG. 7. Highly rectifying *j*-*V* characteristic for the sample: glass/AZO(210)/ZnO(100)/ NiO(20)/Au(400).

as illustrated from the highly rectifying *j*-*V* characteristic in Fig. 7, measured for the sample: glass/AZO(210)/ZnO(100)/NiO(20)/Au(400).

We have investigated the electrical transport characteristics of the heterojunctions in dark and under AM1.5 G (1 kW/m^2) illumination. For this, 400 nm-thick Au contacts were sputter-deposited through a shadow mask on top of the glass/AZO(210)/ZnO(100)/CuO(x)/NiO(20) multilayers. Individual solar cells were contacted with indium-gold wires, as shown in Fig. 8(a). Fig. 8(b) shows the j-V characteristics obtained, as a function of the CuO thickness, for $x = 400$, 500, 600, and 900 nm. Application of forward bias voltage across the heterojunction leads to electron flow from the n-type ZnO to the p-type CuO. The current density value at $+1$ V over its value at -1 V defines the rectification at this bias voltage, which is in the order of 10 for the investigated heterojunctions. The rectification increases for larger bias, assuming values over 100 for a bias of 2 V. Under illumination, maximum short circuit current density of $j_{sc} = 0.85$ mA/cm^2 is obtained for $x = 500$ nm. Thinner or thicker absorber films lead to a decrease of j_{sc} (see Fig. 7(b)). In parallel, the open circuit voltage, V_{oc}, constantly declines from a value of 400 mV for $x = 400$ nm to 210 mV for $x = 900$ nm. The fill factor (FF) also maximizes for $x = 500$ nm at 27.2%. Finally, the power conversion efficiency assumes a maximum of $\eta = 0.08\%$ for $x = 500$ nm. This value is on par with the best efficiency reported in the literature for CuO absorber, in a cell composed of CuO nanowires, thermally grown from a Cu sheet, and then coated with ZnO.[21] We would also like to point out the effect of NiO in the PV characteristics. Its presence as an anode interfacial layer was found to enhance both j_{sc} and V_{oc}. More specifically, for solar cells with $x = 500$ nm, the employment of 20 nm NiO gave rise to an almost 2-fold increase of j_{sc} and an increase of the V_{oc} by up to 120 mV. The origin of this large improvement is at the moment under investigation. Nevertheless, it is possible that NiO, due to its low electron affinity value (see Fig. 6), blocks electrons from migrating to the top electrode, thereby preventing recombination at the top electrode's proximity and enhancing the overall PV efficiency. In addition, it may provide a certain passivation of the CuO surface against ambient conditions.

The aforementioned behavior of the j_{sc} and V_{oc} as a function of the absorber thickness suggests that the carrier collection efficiency is the major cause for the reduced PV performance. First, from optical measurements, we extracted that the average visible light (380–750 nm) transmission through the whole multilayer incorporating 900 nm of CuO (excluding the Au contact) is 4.8% and the infrared light (750–1000 nm) transmission is 51%. The light is therefore not completely absorbed, even for the thickest CuO film. We would therefore expect j_{sc} to increase with the absorber thickness in the investigated x window. This would apply on the assumption that the carrier diffusion length, L, in CuO is long enough for the generated carriers to be collected at their respective electrodes. It is therefore essential to estimate L, which is

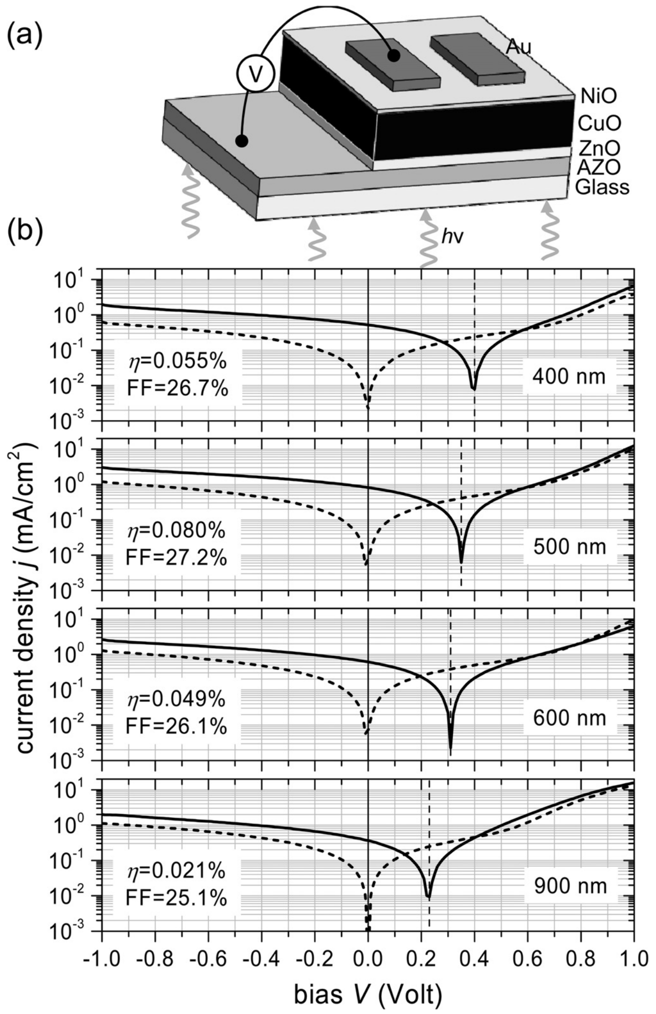

FIG. 8. (a) Schematic representation of the solar cell design. (b) *j-V* characteristics in dark and under illumination for solar cells with different CuO thickness.

connected to the carrier mobility, μ, and lifetime, τ, through the relation: $L = (\tau\mu kT)^{1/2}$, where k is Boltzmann's constant and T is the temperature.

The carrier lifetime for the CuO film was determined from pump-probe transient absorption experiments. A 532 nm laser pulse was used to pump electron-hole pairs into the film following absorption. A probe pulse from a 1064 nm laser arrived at the sample at a variable time following the pump and the differential absorption of the sample, related to the carrier population, was monitored as a function of the delay time. The measurement is shown in Fig. 9, where $\Delta\alpha/\alpha$ is the absorption differential between the on- and off-state of the pump beam, divided by the absorption at the off-state. The experimental data could be fitted with a bi-exponential curve, yielding two characteristic decay time constants for the carrier population in the CuO film: $\tau_1 = 40$ ps and $\tau_2 = 460$ ps.

Band structure calculations for CuO predict high electron and hole effective masses.[31] Indeed, the longitudinal and transverse electron effective masses were reported $0.78m_0$ and $3.52m_0$, respectively (m_0 the rest mass of the free electron), whereas the average hole effective mass was found $1.87m_0$.[31] These values are much larger compared to Si, whose effective masses are $0.26m_0$ and $0.39m_0$ for electrons and holes, respectively. As a result, the carrier mobilities in CuO are expected to be significantly smaller than Si. Hall measurements were conducted on single CuO films sputtered on glass, in the van der Pauw geometry. A hole carrier

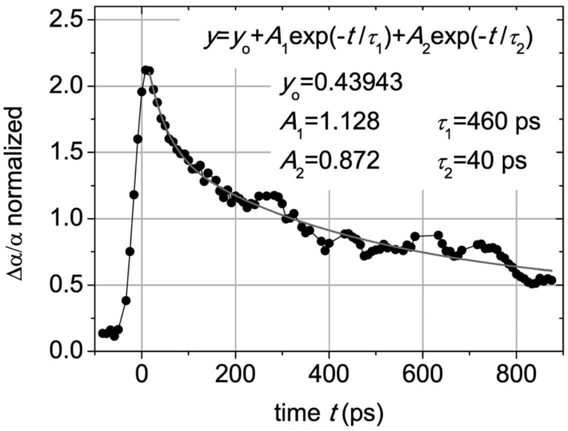

FIG. 9. Transient absorption measurement with the fitting for the extraction of the carrier lifetime in a CuO layer on glass.

concentration of $7.5 \times 10^{16}\,\mathrm{cm}^{-3}$ and hole mobility of 3.45 cm^2/Vs were extracted. This mobility value, combined with the experimental carrier lifetime of 460 ps, results in a carrier diffusion length of approximately 40 nm, i.e., much smaller than the absorber thickness for all investigated solar cells. This strongly suggests a limited efficiency for charge carrier collection. Moreover, in the presented solar cell, illumination takes place through the glass substrate. Higher energy photons are absorbed closer to the ZnO/CuO junction and electron-hole pairs are generated. At the junction proximity, electrons are separated from holes and readily evacuated towards the AZO bottom contact. On the other hand, carriers which are generated further inside the absorber, due to the restricted diffusion length, recombine before reaching their respective electrodes and therefore do not contribute in the extracted current. It is now essential to note that, for sufficiently thin CuO films, a large portion of the non-absorbed light will be reflected at the Au top contact and reenter the absorber, increasing the absorption path and, most importantly, creating carriers at the junction proximity, where they can be collected. This gives rise to larger current. There is, therefore, an optimum absorber thickness for maximizing the extracted current, which is around 500 nm. Below this thickness, the current decreases because of less light absorption and above this thickness because a part of the photo-generated carriers cannot be collected. The enhanced recombination for thicker absorber layers will also cause the observed reduction of the open circuit voltage.

It is therefore concluded that the ZnO/CuO heterojunction PV performance is compromised by the poor carrier lifetime in CuO. However, the material can be still promising in extremely thin absorber (ETA) solar cells, combined, for example, with ZnO nanorods.[37] In that case, the decoupling of the light absorption and carrier collection paths to orthogonal directions could permit decent solar cell performance despite the poor electronic properties.

In summary, we have demonstrated PV activity from sputtered, thin film heterojunctions combining p-type CuO absorber with n-type ZnO. The efficiency, the short circuit current, and the open circuit voltage were found to depend on the CuO thickness, with maximum efficiency of 0.08%, obtained for a thickness of 500 nm. These dependencies can be explained by the limited carrier collection efficiency, stemming from the small carrier lifetime in CuO. The carrier population was found to decay with time constants of 40 and 460 ps. CuO has potential as an abundant, low environmental impact absorber in solar cell architectures where extremely thin absorber layers are employed.

ACKNOWLEDGMENTS

We would like to acknowledge financial support from the Austrian "Klima und Energie Fonds" through the project "SANCELL."

[1] C. Wadia, A. P. Alivisatos, and D. M. Kammen, Environ. Sci. Technol. **43**, 2072 (2009).
[2] F. Alharbi, J. D. Bass, A. Salhi, A. Alyamani, H.-C. Kim, and R. D. Miller, Renewable Energy **36**, 2753 (2011).
[3] L. C. Olsen, F. W. Addis, and W. Miller, Sol. Cells **7**, 247 (1982).
[4] A. Mittiga, E. Salza, F. Sarto, M. Tucci, and R. Vasanthi, Appl. Phys. Lett. **88**, 163502 (2006).
[5] T. Minami, T. Miyata, K. Ihara, Y. Minamino, and S. Tsukada, Thin Solid Films **494**, 47 (2006).
[6] M. Izaki, T. Shinagawa, K. T. Mizuno, Y. Ida, M. Inaba, and A. Tasaka, J. Phys. D: Appl. Phys. **40**, 3326 (2007).
[7] T. Minami, Y. Nishi, T. Miyata, and J. Nomoto, Appl. Phys. Express **4**, 62301 (2011).
[8] Y. Nakamura, A. Ando, T. Tsurutami, O. Okada, M. Miyayama, K. Koumoto, and H. Yanagida, Chem. Lett. **15**, 413 (1986).
[9] Y. Nakamura, H. Yoshioka, M. Miyayama, H. Yanagida, and T. Tsurutani, J. Electrochem. Soc. **137**, 940 (1990).
[10] K. Hikita, M. Miyayama, and H. Yanagida, J. Ceram. Soc. Jpn. **102**, 810 (1994).
[11] S. Ayguen and D. Cann, Sens. Actuators B **106**, 837 (2005).
[12] K. H. Yoon, W. J. Choi, and D. H. Kang, Thin Solid Films **372**, 250 (2000).
[13] Y. S. Chaudhary, A. Agrawal, R. Shrivastav, V. R. Satsangi, and S. Dass, Int. J. Hydrogen Energy **29**, 131 (2004).
[14] D. Chauhan, V. R. Satsangi, S. Dass, and R. Shrivastav, Bull. Mater. Sci. **29**, 709 (2006).
[15] S. Anandan, X. Wen, and S. Yang, Mater. Chem. Phys. **93**, 35 (2005).
[16] Y. Bar-Yam, Phys. Rev. B **43**, 2601 (1991).
[17] J. B. Goodenough, J. S. Zhou, and J. Chan, Phys. Rev. B **47**, 5275 (1993).
[18] Y. F. Lim, J. J. Choi, and T. Hanrath, J. Nanomater. **2012**, 393160.
[19] Q. Bao, C. M. Li, L. Liao, H. Yang, W. Wang, C. Ke, Q. Song, H. Bao, T. Yu, K. P. Loh, and J. Guo, Nanotechnology **20**, 065203 (2009).
[20] R. Motoyoshi, T. Oku, H. Kidowaki, A. Suzuki, K. Kikushi, S. Kikushi, and B. Jeyadevan, J. Ceram. Soc. Jpn. **118**, 1021 (2010).
[21] P. Wang, X. Zhao, and B. Li, Opt. Express **19**, 11271 (2011).
[22] M. Neuschitzer, A. Moser, A. Neuhold, J. Kraxner, B. Stadlober, M. Oehzelt, I. Salzmann, R. Resel, and J. Novak, J. Appl. Crystallogr. **45**, 367 (2012).
[23] See http://www.mindat.org/min-3912.html for a crystallographic description of tenorite.
[24] See http://rruff.geo.arizona.edu/doclib/hom/tenorite.pdf for the morphological features of the tenorite crystal.
[25] R. W. Smith and D. J. Srolovitz, J. Appl. Phys. **79**, 1448 (1996).
[26] I. C. Madsen, N. V. Y. Scarlett, L. M. D. Cranswick, and T. Lwin, J. Appl. Cryst. **34**, 409 (2001).
[27] R. J. Powell and W. E. Spicer, Phys. Rev. B **2**, 2182 (1970).
[28] S. Hüfner, Adv. Phys. **43**, 183 (1994).
[29] P. S. Patil and L. D. Kadam, Appl. Surf. Sci. **199**, 211 (2002).
[30] F. P. Koffyberg and F. A. Benko, J. Appl. Phys. **53**, 1173 (1982).
[31] D. Wu, Q. Zhang, and M. Tao, Phys. Rev. B **73**, 235206 (2006).
[32] A. Parretta, M. K. Jayaraj, A. Di Nocera, S. Loreti, L. Quercia, and A. Agati, Phys. Stat. Solidi A **155**, 399 (1996).
[33] J. F. Pierson, A. Thobor-Keck, and A. Billard, Appl. Surf. Sci. **210**, 359 (2003).
[34] I. M. Chan, T. Y. Hsu, and F. C. Hong, Appl. Phys. Lett. **81**, 1899 (2002).
[35] M. D. Irwin, D. B. Buchholz, A. W. Hains, R. P. H. Chang, and T. J. Marks, PNAS **105**, 2783 (2008).
[36] Z. Sun, C. Wang, J. Yang, B. Zhao, and J. R. Lombardi, J. Phys. Chem. C **112**, 6093 (2008).
[37] A. Peić, T. Dimopoulos, R. Resel, S. Abermann, M. Postl, E. J. W. List, and H. Brückl, J. Nanomater. **2012**, 457904.